

Electronic Supplementary Information

Visible to Near-Infrared Plasmon-Enhanced Catalytic Activity of Pd Hexagonal Nanoplates for the Suzuki Coupling Reaction

T. Thuy Trinh,^{*} Ryota Sato, Masanori Sakamoto, Yoshifumi Fujiyoshi, Mitsutaka Haruta, Hiroki Kurata, and Toshiharu Teranishi^{*}

Institute for Chemical Research, Kyoto University, Gokasho Uji, Kyoto 611-0011, Japan

^{*}e-mail: trinh.thangthuy.8m@kyoto-u.ac.jp; teranisi@scl.kyoto-u.ac.jp

Contents	Page
A. Experimental Information	2
B. Calculations of the Total Number of Surface Pd Atoms	4
Fig. S1. TEM images of Pd NPs synthesized in the presence of PVP (PVP/Pd molar ratio: 9.6/1) and the absence of formaldehyde at 80 °C	7
Fig. S2. TEM images of Pd NPs synthesized in the presence of PVP (PVP/Pd molar ratio: 5/1) and the absence of formaldehyde at 80 °C	7
Fig. S3. TEM images of Pd NPs synthesized in the presence of PVP (PVP/Pd molar ratio: 9.6) and the absence of formaldehyde at 40 °C	7
Fig. S4. Size and shape evolution of Pd hexagonal nanoplates synthesized in the presence of PVP (PVP/Pd molar ratio: 9.6/1) and formaldehyde at 40 °C	8
Fig. S5. Edge lengths l_1 , crystalline sizes and UV-vis-NIR absorption spectra of Pd hexagonal nanoplates synthesized in the presence of PVP (PVP/Pd molar ratio: 9.6/1) and formaldehyde at 40 °C.	8
Fig. S6. TEM, Cs-corrected HRTEM images and NBD pattern of individual Pd hexagonal nanoplate obtained along the $\langle 112 \rangle$ axis.	9
Fig. S7. TEM, HRTEM images and side length distributions of Pd octahedra and nanocubes, and optical properties of hex-Pd, oct-Pd and cub-Pd.	9
Fig. S8. TGA/DTA of hex-Pd, oct-Pd and cub-Pd	10
Fig. S9. Schematic illustration of the Pd hexagonal nanoplate and its deconvoluted structures, and size distributions of the Pd hexagonal nanoplates synthesized over 120h.	11
Fig. S10. Instrumentation for Suzuki coupling reactions carried out under Xenon illumination	12
Fig. S11. Catalytic activity of hex-Pd was compared with oct-Pd and cub-Pd in Suzuki coupling reactions carried out under Xenon illumination	12
Fig. S12. Time-dependent temperature profiles of the Suzuki coupling reaction solutions	13
Fig. S13. TEM images of Pd NPs before and after the Suzuki coupling reactions	13
Fig. S14. Simulated absorption cross section spectra for longitudinal mode of individual regular Pd hexagonal prisms	14
References	14

A. Experimental Information

Chemicals. Sodium tetrachloropalladate (II) (Na_2PdCl_4 , purity 98%), polyvinylpyrrolidone (PVP, Mw 55000), formaldehyde solution 37 wt%, *L*-ascorbic acid (purity >99%), potassium bromide (KBr, purity >99%) and phenylboronic acid (purity 95%) were purchased from Sigma Aldrich Corp. Iodobenzene was purchased from Kanto Chemical Co., Inc. Potassium carbonate (K_2CO_3 , purity 99.5%) was purchased from Wako Pure Chemical Industries, Ltd. All reagents were used without further purification.

Mechanism for the synthesis of Pd hexagonal nanoplates. The wet-chemical synthesis of polyhedral metal nanoparticles (NPs) relies on either thermodynamically or kinetically controlled process. The thermodynamically controlled synthesis preferentially produces stable structures with low surface energies. For a face-centered cubic (*fcc*) structure, the surface energies of low-index crystallographic facets that typically encase a NP are in the order of $\gamma\{111\} < \gamma\{100\} < \gamma\{110\}$. The surface energy of facet can be altered by introducing capping agents through their interaction with facet. The kinetically controlled synthesis can produce less stable structures deviated from thermodynamics. The kinetic control for the synthesis of polyhedral metal (Au, Ag, Pt and Pd) nanoplates can be achieved by sufficiently slow reduction of metallic precursors.¹ The process usually involves the formation of seeds through random hexagonal close packing of metal atoms, which leads to form plate-like seeds enclosed by $\{111\}$ facets at the top and bottom surfaces with stacking faults.¹ The seeds further grow to form metal nanoplates with their top and bottom faces enclosed by $\{111\}$ facets and the side surfaces surrounded by a mixture of $\{111\}$ and $\{100\}$ facets. The seeds firstly grow into plates with a hexagonal cross-section due to the six-fold symmetry of an *fcc* structure, and can further grow into triangular cross-section plates by eliminating $\{111\}$ facets from the side surfaces.¹ For the synthesis of Pd hexagonal nanoplates, one has to suppress the elimination of side $\{111\}$ facets.

PVP terminated in the hydroxyl group has been found to serve as a mild reducing agent for the kinetically controlled synthesis of Pd nanoplates in an aqueous solution containing Na_2PdCl_4 .²⁻⁴ As a result, the aqueous synthesis of Pd nanoplates using only PVP could rationally control the formation of Pd hexagonal and triangular nanoplates in a small scale reaction with a Na_2PdCl_4 concentration of 7 mM and a volume of 11 mL at 80 °C. However, dimension of the Pd nanoplates stays untouched from this synthesis.² This reaction when the concentration of Na_2PdCl_4 was scaled up to 32 mM was confirmed to produce a high fraction of triangle to hexagon at 80 °C (Figs S1 and S2) and complex structures including nanoplates, nanoprism and other many irregular shapes at 40 °C (Fig. S3). Therefore, the large scale and dimension controlled synthesis of Pd hexagonal nanoplates requires further controlled parameters.

We thereby introduced formaldehyde in the reaction and expected to further alter the surface energy of Pd plate-like seeds and, thus keep the kinetic growth in a long period of time.^{1,3,4} It has been found that PVP and formaldehyde have selective interactions with $\{100\}$ and $\{111\}$ facets, respectively.^{1,3,5} Therefore, the use of formaldehyde is also expected to suppress the elimination of $\{111\}$ side surfaces in the growth stage, resulting in the formation of Pd hexagonal nanoplates. Indeed, a reaction of Na_2PdCl_4 (32 mM) in a volume of 500 mL in the presence of PVP (154.8 mmol calculated for a PVP monomer with a molecular weight of 111 g/mol) and formaldehyde (219.8 mmol) at 40°C produced relatively monodispersed NPs with a plate-like shape and a circular size of 4.6 ± 1.7 nm after 3 h (Fig. S4A). These Pd plate-like NPs are regarded as seeds for the further kinetic growth to form Pd hexagonal nanoplates (Fig. S4B-G). In this synthesis, we could control over the edge length of Pd hexagonal nanoplates by changing reaction time (Fig. S5A). The average edge lengths l_1 were estimated from at least 500 nanoplates using TEM images (Fig. S4B-G) to be 31.7 ± 10.5 , 34.3 ± 12.5 , 44.8 ± 18.7 , 57.5 ± 19.3 , 59.9 ± 20.8 , and 60.4 ± 19.3 nm corresponding to the reaction times of: 12, 24, 48, 72, 96, and 120 h, respectively (Fig. S5A). To estimate the thickness of Pd hexagonal nanoplates, we prepared TEM sample by dropping a dispersion of highly concentrated and well-washed nanoplates on carbon grid, which leads to the assembly of nanoplates into an extended lamellar structure (Fig. 1B, Main Text). The thickness of Pd hexagonal nanoplates synthesized over 120 h was estimated using TEM images to be 20.5 nm. XRD patterns of the as-synthesized Pd hexagonal nanoplates exhibited a typical *fcc* crystal structure and a dominance of the (111) diffraction peak (Fig. S4H). The mean crystalline sizes (D_{XRD}) of Pd hexagonal nanoplates, which were estimated from the (111) diffraction peaks (Fig. S4I) using the Scherrer formula, varied from 16.1 to 19.6 nm with increasing reaction time from 12 to 120 h (Fig. S5A). This is almost unchanged with increasing reaction time. It is worth to note that the as-synthesized Pd hexagonal nanoplates tend to lie in a planar fashion on XRD substrate by dropping their dispersion in ethanol on a glass substrate (Fig. S4G). In addition, the mean crystalline size of Pd hexagonal nanoplates synthesized over 120 h (19.6 nm) is similar to their corresponding average thickness estimated from TEM images (20.5 nm). Therefore, the mean crystalline size could be regarded as the thickness of Pd hexagonal nanoplates and it could not be controlled by changing reaction time. It is clear that formaldehyde plays an important role in the formation of Pd hexagonal nanoplates in a gram-scale synthesis with a relatively high product yield and high shape

selectivity. This presumably comes from the selective adsorption of formaldehyde onto {111} facets of the Pd hexagonal nanoplates, which can suppress the elimination of {111} side surfaces. The strong interaction of formaldehyde with the {111} top and bottom faces of Pd hexagonal nanoplates can inhibit a further addition of Pd atoms on these faces, resulting in the unchanged thickness with increasing reaction time.

Synthesis of Pd Nanocubes. The synthesis of Pd nanocubes followed the method reported by Jin and co-worker with some modification.⁶ PVP (2.8 g, 25 mmol) and ascorbic acid (0.66 g, 3.75 mmol) were dissolved in miliQ water (250 mL) in a 300 mL three-neck flask by magnetic stirring for 1 h, and the solution was heated to 80 °C for 1 h. An aqueous solution prepared by dissolving Na₂PdCl₄ (1.47 g, 5 mmol) and KBr with different amounts in miliQ water (50 mL) was then added into the flask. The reaction was allowed to proceed at 80°C for 3 h in air. The final product was washed with five times with a mixture of ethanol and acetone (1:4, v/v) and collected by centrifugation each time. For Suzuki coupling reaction, the as-synthesized nanocubes were further efficiently washed with ethanol. The cubic shape, the {100}-bound surface structure and size distribution of the synthesized NPs were confirmed by SEM, TEM and HRTEM, as shown in Fig. S7D-F. The particle sizes were estimated from TEM images to be $9.7 \pm 1.4 \times 8.2 \pm 1.2$ nm and $14.8 \pm 1.7 \times 13.1 \pm 1.3$ nm, corresponding to the KBr amounts of 7.9 g (66.5 mmol) and 15.8 g (133 mmol), respectively. The reaction yield for the later synthesis was estimated using TGA (Fig. S8C) to be 90%.

Synthesis of Pd Octahedra. The synthesis of Pd octahedral followed the method reported by Jin and co-worker with some modification.⁵ PVP capped Pd nanocube seeds with a particle size of $9.7 \pm 1.4 \times 8.2 \pm 1.2$ nm (32 mg, 0.3 mmol, based on Pd content), PVP (5.7 g, 51.6 mmol) and formaldehyde solution 37 wt% (8.2 mL, 109.9 mmol) were dissolved in milliQ water (500 mL) in a 1 L three-neck flask by magnetic stirring for 1 h, and the solution was heated to 40°C for 1 h. An aqueous solution of Na₂PdCl₄ (1.58 g, 5.4 mmol) in milliQ water (100 mL) was then added into the flask. The reaction was allowed to proceed at 40 °C for 24 h in air. The final product was washed with five times with a mixture of ethanol and acetone (1:3, v/v) and collected by centrifugation each time. For Suzuki coupling reaction, the as-synthesized octahedra were further efficiently washed with ethanol. The octahedral shape, the {111}-bound surface structure and size distribution of the synthesized NPs were confirmed by SEM, TEM and HRTEM, as shown in Fig. S7A-C. The edge length of Pd nanooctahedra was estimated from TEM images to be 15.7 ± 2.3 nm. The reaction yield was estimated using TGA (Fig. S8B) to be 92%.

Structural Characterization and Elemental Analyses. Transmission electron microscopy (TEM) analysis was performed on a JEOL JEM-1011 transmission electron microscope operated at the accelerating voltage of 100 kV. Spherical aberration corrected high resolution TEM (Cs-corrected HRTEM), selected area electron diffraction (SAED) and nano-beam diffraction (NBD) analyses were performed on a JEOL JEM-2200FS transmission electron microscope equipped with a Cs corrector and operated at the accelerating voltage of 200 kV. SAED and NBD patterns were calibrated using the lattice spacing of a polycrystalline Au sample. Spherical aberration corrected high-angle annular dark-field scanning TEM (Cs-corrected HAADF-STEM) analysis was performed on a JEOL JEM-9980TKP1 scanning transmission electron microscope equipped with a Cs corrector and operated at the accelerating voltage of 200 kV. The probe convergence angle was 23 mrad, and the inner detector angle was 70-170 mrad. Field emission scanning electron microscopy (FESEM) analysis was performed on a Hitachi S-4800 scanning electron microscope. TEM and SEM samples were prepared by dropping a dispersion of NPs in ethanol onto a carbon coated copper grid or silicon wafer and drying in air. X-ray diffractometry (XRD) patterns were collected in reflection geometry using a PANalytical X'Pert Pro MPD power X-ray diffractometer at room temperature with Cu K α radiation ($\lambda = 1.542$ Å). XRD samples were prepared by dropping a dispersion of NPs in ethanol onto a glass substrate and drying in air. UV-Vis-NIR absorption spectra were recorded on a Hitachi U-4100 spectrophotometer. Thermogravimetry (TG) was performed on a Shimadzu DTG-60. Gas chromatography coupled with a mass spectroscopic detector (GCMS) analysis was performed on a Shimadzu GCMS-QP5050 gas chromatography mass spectrometer. Inductively coupled plasma atomic emission spectroscopy (ICP-AES) analysis was performed on a ICPE-9820 (Frequency 27 MHz) with a detection limit (LD) of 3 ppb and quantification detection limit (LQD) of 10 ppb operated at the radio frequency power of 1.40 kW and the Ar plasma gas flow rate of 18.0 L/min. All samples for ICP-AES analysis are in ethanol.

Instrumentation and Conditions for Suzuki Coupling Reactions. Instrumentation and conditions for Suzuki coupling reactions under light illumination are illustrated in Fig. S10. The light source is a Xenon Arc Lamp (MAX 303, ASAHI) with three optical filters including 350 nm, 380 nm and >420 nm bandpass filters. The heat absorbing filter (HAF-50S-50H, SIGMAKOKI) was also used to keep away the heat that liberate from the NIR and IR range and cut off the brightness of the NIR and IR light, as well as cut off spot light that liberate heat in microscope illumination. The typical transmittance

spectrum of the heat absorbing filter is 300 – 1000 nm (Fig. S10). The final light sources that irradiated on reaction solutions are therefore approximately $\lambda = 350, 380, 420 - 1000$ and 300 – 1000 nm.

B. Calculations of the Total Number of Surface Pd Atoms

Pd hexagonal nanoplates

The number of surface Pd atoms in a single Pd hexagonal nanoplate. The structure of the Pd hexagonal nanoplate is illustrated in Fig. S9A. Its dimensions including two edge lengths (l_1 and l_2), the thickness (h_1) and side heights (h_2 and h_3) were estimated from TEM images and are shown in Fig. S9D.

The Pd hexagonal nanoplate is deconvoluted into four basic shapes and composed of one regular hexagonal prism, six triangular prisms, six triangular pyramids and twelve rectangular pyramids, as seen in Fig. S9A. The total volume V of Pd hexagonal nanoplate is expressed as:

$$V = \frac{3\sqrt{3}}{2}AB^2 \times AG + 6V_{\text{DJKEIL}} + 6V_{\text{GAEF}} + 12V_{\text{EAGLI}} \quad (1).$$

$$\text{The volume of regular hexagonal prism is } \frac{3\sqrt{3}}{2}AB^2 \times AG = \frac{3\sqrt{3}}{2}l_1^2 \times h_1 = 1.94 \times 10^5 \text{ nm}^3 \quad (2).$$

V_{DJKEIL} is the volume of triangular prism DJKEIL and expressed as: $V_{\text{DJKEIL}} = DE \times A_{\text{EIL}}$ (3), where A_{EIL} is the area of triangle EIL and calculated using Heron's formula:

$$A_{\text{EIL}} = \frac{1}{4}\sqrt{(IL + EI + EL)(-IL + EI + EL)(IL - EI + EL)(IL + EI - EL)} \quad (4).$$

Substituting (4) into (3), the volume of triangular prism DJKEIL is

$$\begin{aligned} V_{\text{DJKEIL}} &= DE \times \frac{1}{4}\sqrt{(IL + EI + EL)(-IL + EI + EL)(IL - EI + EL)(IL + EI - EL)} \\ &= \frac{1}{4}l_2\sqrt{(h_1 + h_2 + h_3)(-h_1 + h_2 + h_3)(h_1 - h_2 + h_3)(h_1 + h_2 - h_3)} = 1.78 \times 10^3 \text{ nm}^3 \end{aligned} \quad (5).$$

V_{GAEF} is the volume of triangular pyramid GAEF and expressed as: $V_{\text{GAEF}} = \frac{1}{3}GV \times A_{\text{AEF}}$ (6), where GV is the height of triangular pyramid GAEF at the apex G and expressed as: $GV = GA \times \sin(\angle GAV)$. GV is perpendicular to the plane AEF. Thus, GV is perpendicular to AB because AB is in the plane AEF. In addition, AB is perpendicular to GA . Therefore, AB is perpendicular to the plane GAV, and is thus perpendicular to AV . AV and GA are perpendicular to AB , therefore angle GAV ($\angle GAV$) is the angle between the plane ABHG and the plane ABCDEF. This is the angle between the plane ABHG and a side $\{111\}$ facet and expressed as: $\angle GAV = \angle(111, -1 - 11) - 90^\circ = 109.47^\circ - 90^\circ = 19.47^\circ$, where $\angle(111, -1 - 11) = 109.47^\circ$ is the angle between the (111) and $(-1 - 11)$ facets. So $GV = h_1 \times \sin(19.47^\circ) = 6.8 \text{ nm}$ (7). A_{AEF} is the area of triangle AEF and calculated using Heron's formula:

$$A_{\text{AEF}} = \frac{1}{4}\sqrt{(AE + AF + EF)(-AE + AF + EF)(AE - AF + EF)(AE + AF - EF)} \quad (8).$$

$$\text{Where: } AE = \sqrt{EI^2 + AI^2} = \sqrt{EI^2 + \left(\frac{AB-ED}{2}\right)^2} = \sqrt{h_2^2 + \left(\frac{l_1-l_2}{2}\right)^2} = 15.3 \text{ nm} \quad (9).$$

$$AF = \sqrt{FM^2 + AM^2} = \sqrt{FM^2 + \left(\frac{AB-ED}{2}\right)^2} = \sqrt{h_3^2 + \left(\frac{l_1-l_2}{2}\right)^2} = 6.7 \text{ nm} \quad (10).$$

$$EF = \sqrt{ES^2 + FS^2} \quad (11).$$

Where

$$\begin{aligned} FS &= FQ + QR + RS = FP \times \sin(\angle FPQ) + NO + AI = EU \times \sin(\angle IAM - 90^\circ) + NO + AI \\ &= (NO + AI) \times \sin(120^\circ - 90^\circ) + NO + AI = (NO + AI) \times (\sin(30^\circ) + 1) \end{aligned}$$

$$\begin{aligned}
&= \left(\frac{AO}{\tan(\angle ANO)} + AI \right) \times (\sin(30^\circ) + 1) = \left(\frac{AO}{\tan\left(\frac{\angle IAM}{2}\right)} + AI \right) \times (\sin(30^\circ) + 1) \\
&= \left(\frac{AT \times \cos(\angle OAT)}{\tan\left(\frac{\angle IAM}{2}\right)} + AI \right) \times (\sin(30^\circ) + 1) = \left(\frac{EI \times \cos(\angle(-111, -1 - 11))}{\tan\left(\frac{\angle IAM}{2}\right)} + AI \right) \times (\sin(30^\circ) + 1) \\
&= \left(\frac{EI \times \cos(70.53^\circ)}{\tan(60^\circ)} + \frac{AB - ED}{2} \right) \times (\sin(30^\circ) + 1) = \left(\frac{h_2 \times \cos(70.53^\circ)}{\tan(60^\circ)} + \frac{l_1 - l_2}{2} \right) \times (\sin(30^\circ) + 1) \\
&= 7.3 \text{ nm} \tag{12},
\end{aligned}$$

$$\begin{aligned}
ES &= EI - SI = EI - RA = EI - \sqrt{AF^2 - FR^2} = EI - \sqrt{AF^2 - (FS - RS)^2} = EI - \sqrt{AF^2 - (FS - AI)^2} \\
&= h_2 - \sqrt{6.7^2 - \left(7.3 - \frac{l_1 - l_2}{2}\right)^2} = 11.2 \text{ nm} \tag{13}.
\end{aligned}$$

Where $\angle(-111, -1 - 11) = 70.53^\circ$ is the angle between the (-111) and $(-1 - 11)$ facets.

$$\text{Substituting (12) and (13) into (11), } EF = 13.4 \text{ nm} \tag{14}.$$

$$\text{Substituting (9), (10) and (14) into (8), } A_{AEF} = 4.48 \times 10^1 \text{ nm}^2 \tag{15}.$$

$$\text{Substituting (7) and (15) into (6), the volume of triangular pyramid GAEF is } V_{GAEF} = 1.02 \times 10^2 \text{ nm}^3 \tag{16}.$$

V_{EAGLI} is the volume of rectangular pyramid EAGLI and expressed as: $V_{EAGLI} = \frac{1}{3}AO \times A_{AGLI}$ (17). Where $AO = AT \times \cos(\angle OAT) = h_2 \times \cos(70.53^\circ) = 5.1 \text{ nm}$ (18), is the distance between the plane AGLI and the plane NOTU. It is therefore equal to the height of pyramid EAGLI at the apex E. A_{AGLI} is the area of rectangle AGLI and expressed as: $A_{AGLI} = EI \times AI = h_2 \times \frac{l_1 - l_2}{2} = 2.89 \times 10^1 \text{ nm}^2$ (19). Substituting (18) and (19) into (17), the volume of rectangular pyramid EAGLI is $V_{EAGLI} = 4.91 \times 10^1 \text{ nm}^3$ (20).

$$\text{Substituting (2), (5), (16) and (20) into (1), the total volume of a single Pd hexagonal nanoplate is } V = 2.06 \times 10^5 \text{ nm}^3 \tag{21}.$$

The Pd hexagonal nanoplate has two $\{111\}$ planes at the top and bottom faces, six $\{111\}$ planes and six $\{100\}$ planes as the side surfaces. The total area of $\{111\}$ surfaces is the total area of two regular hexagons at the top and bottom faces and six side irregular hexagons and expressed as:

$$A_{\{111\}} = 2 \times \frac{3\sqrt{3}}{2} \times l_1^2 + 6 \times A_{ABCDEF} \tag{22}.$$

Where, A_{ABCDEF} is the area of irregular hexagon ABCDEF and expressed as: $A_{ABCDEF} = A_{ABDE} + 2 \times A_{AEF}$ (23). A_{ABDE} is the area of isosceles trapezoid ABDE and expressed as:

$$A_{ABDE} = \frac{EI \times (AB + DE)}{2} = \frac{h_2 \times (l_1 + l_2)}{2} = 8.89 \times 10^2 \text{ nm}^2 \tag{24}.$$

$$\text{Substituting (15) and (24) into (23), } A_{ABCDEF} = 9.79 \times 10^2 \text{ nm}^2 \tag{25}.$$

$$\text{Substituting (25) into (22), } A_{\{111\}} = 2.48 \times 10^4 \text{ nm}^2 \tag{26}.$$

The total area of $\{100\}$ surfaces is the total area of six side isosceles trapezoids DEGH and expressed as:

$$A_{\{100\}} = 6 \times A_{DEGH} = 6 \times \frac{EL \times (DE + GH)}{2} = 6 \times \frac{h_2 \times (l_1 + l_2)}{2} = 2.25 \times 10^3 \text{ nm}^2 \tag{27}.$$

Pd has a face-centered cubic structure with a lattice constant of $a_0 = 0.389 \text{ nm}$. The areas of two-dimensional unit cell on the (111) and (100) planes are $\frac{\sqrt{3}}{4}(\sqrt{2}a_0)^2 = 1.31 \times 10^{-1} \text{ nm}^2$, and $a_0^2 = 1.51 \times 10^{-1} \text{ nm}^2$, respectively.

Each two-dimensional unit cell on the (111) and (100) contains two Pd atoms. The number of surface Pd atoms of a single Pd hexagonal nanoplate is $\frac{A_{\{111\}}}{1.31 \times 10^{-1}} \times 2 + \frac{A_{\{100\}}}{1.51 \times 10^{-1}} \times 2$ (28). Substituting (26) and (27) into (28), the number of surface Pd atoms of a single Pd hexagonal nanoplate is 4.08×10^5 atoms.

The total number of surface Pd atoms present in one Suzuki coupling reaction. A mass density of Pd is 12.023 g/cm³. The mass of a single hex-Pd with a volume of $V = 2.06 \times 10^5 \text{ nm}^3$ is $2.06 \times 10^5 \times 10^{-21} \text{ cm}^3 \times 12.023 \frac{\text{g}}{\text{cm}^3} = 2.48 \times 10^{-15} \text{ g}$.


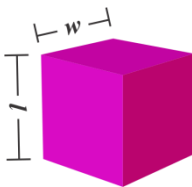
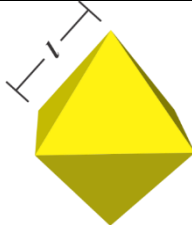
The mass of hex-Pd used for each Suzuki coupling reaction was 0.5 mg. Thus, the total number of hex-Pd in one Suzuki coupling reaction is $\frac{0.5 \times 10^{-3}}{2.48 \times 10^{-15}} = 2.02 \times 10^{11}$.

Finally, the total number of surface Pd atoms in one Suzuki coupling reaction is $4.08 \times 10^5 \times 2.02 \times 10^{11} = 8.24 \times 10^{16}$ atoms.

Pd nanooctahedra and nanocubes

The calculations for oct-Pd and cub-Pd are the same with those for hex-Pd. The results are shown in Table S1. The mass of these NPs used for each Suzuki coupling reaction was 0.5 mg.

Table S1 Geometrical characteristics of oct-Pd and cub-Pd

	Cube	Octahedron
 Shape ■ {111} ■ {100}		
Dimension / nm	$l = 14.8 \pm 1.7$ $w = 13.1 \pm 1.3$	$l = 15.7 \pm 2.3$
The area A of a single NP / nm ²	$A_{(100)} = 2w^2 + 4wl = 1.12 \times 10^3$	$A_{(111)} = 2\sqrt{3}l^2 = 8.54 \times 10^2$
The volume V of a single NP / m ³	$V = w^2l = 2.54 \times 10^3$	$V = \frac{\sqrt{2}}{3}l^3 = 1.82 \times 10^3$
The number of surface Pd atoms in a single NP	1.48×10^4	1.30×10^4
The number of NPs	1.64×10^{13}	2.28×10^{13}
The total number of surface Pd atoms present in one Suzuki coupling reaction	2.43×10^{17}	2.96×10^{17}

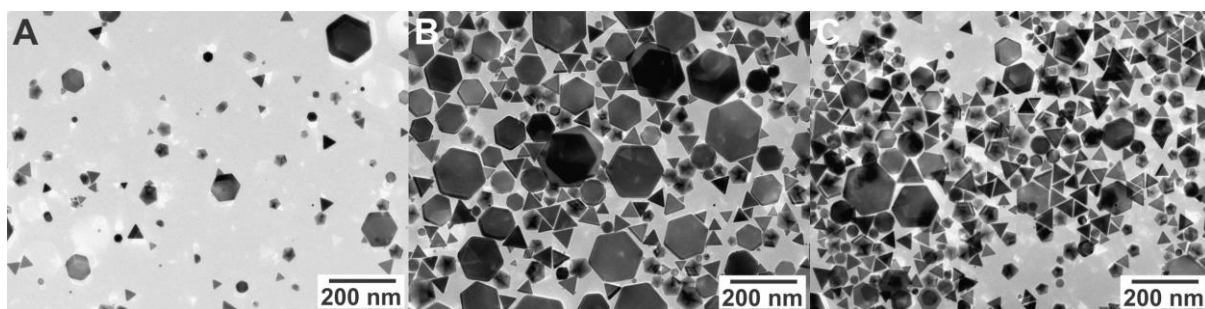


Fig. S1 TEM images of Pd NPs synthesized in the presence of PVP (PVP/Pd molar ratio: 9.6/1) and the absence of formaldehyde at 80 °C for different reaction times (A: 1 h, B: 3 h, and C: 6 h)

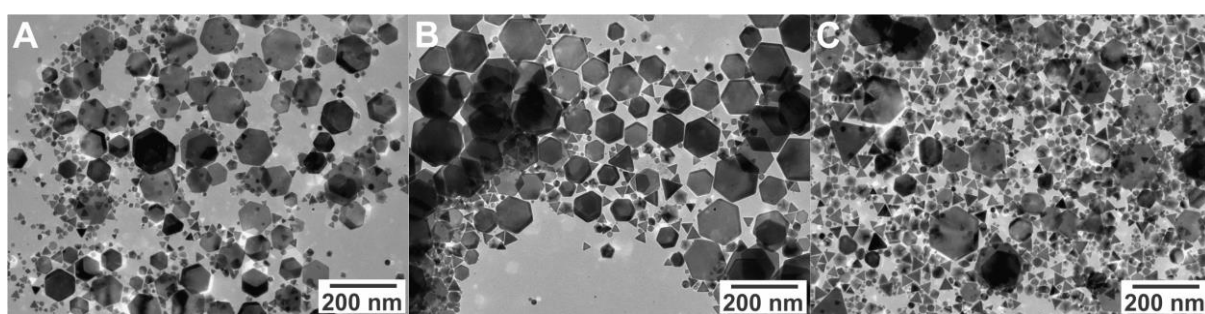


Fig. S2 TEM images of Pd NPs synthesized in the presence of PVP (PVP/Pd molar ratio: 5/1) and the absence of formaldehyde at 80 °C for different reaction times (A: 1 h, B: 3 h, and C: 6 h).

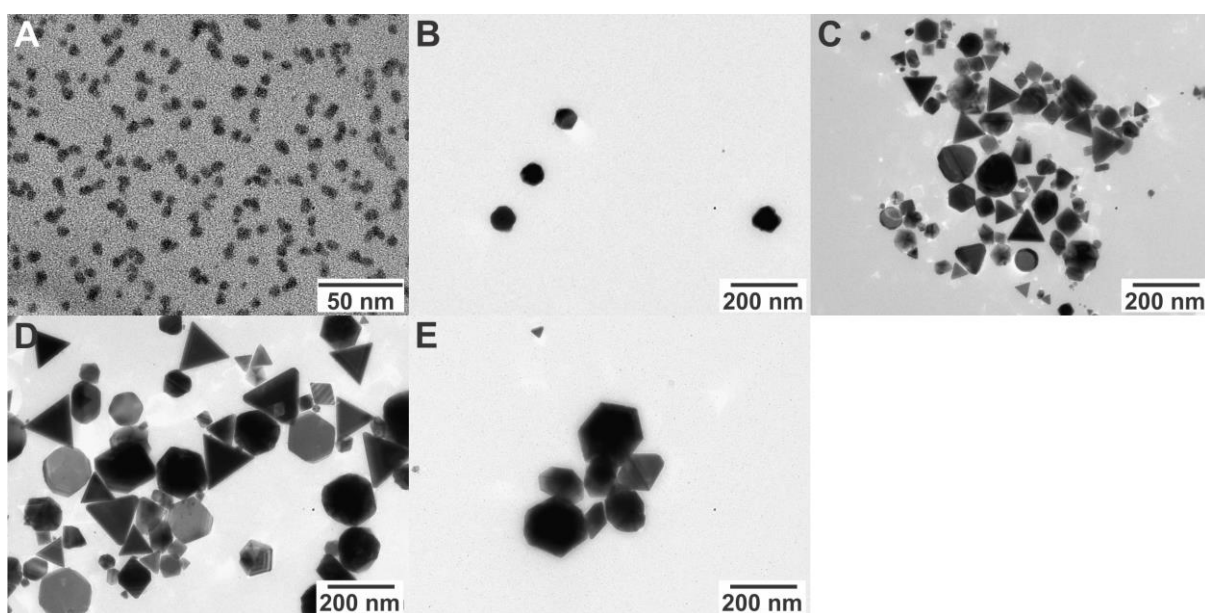


Fig. S3 TEM images of Pd NPs synthesized in the presence of PVP (PVP/Pd molar ratio: 9.6) and the absence of formaldehyde at 40 °C for different reaction times (A: 1 h, B: 3 h, C: 6 h, D: 24 h, and E: 48 h)

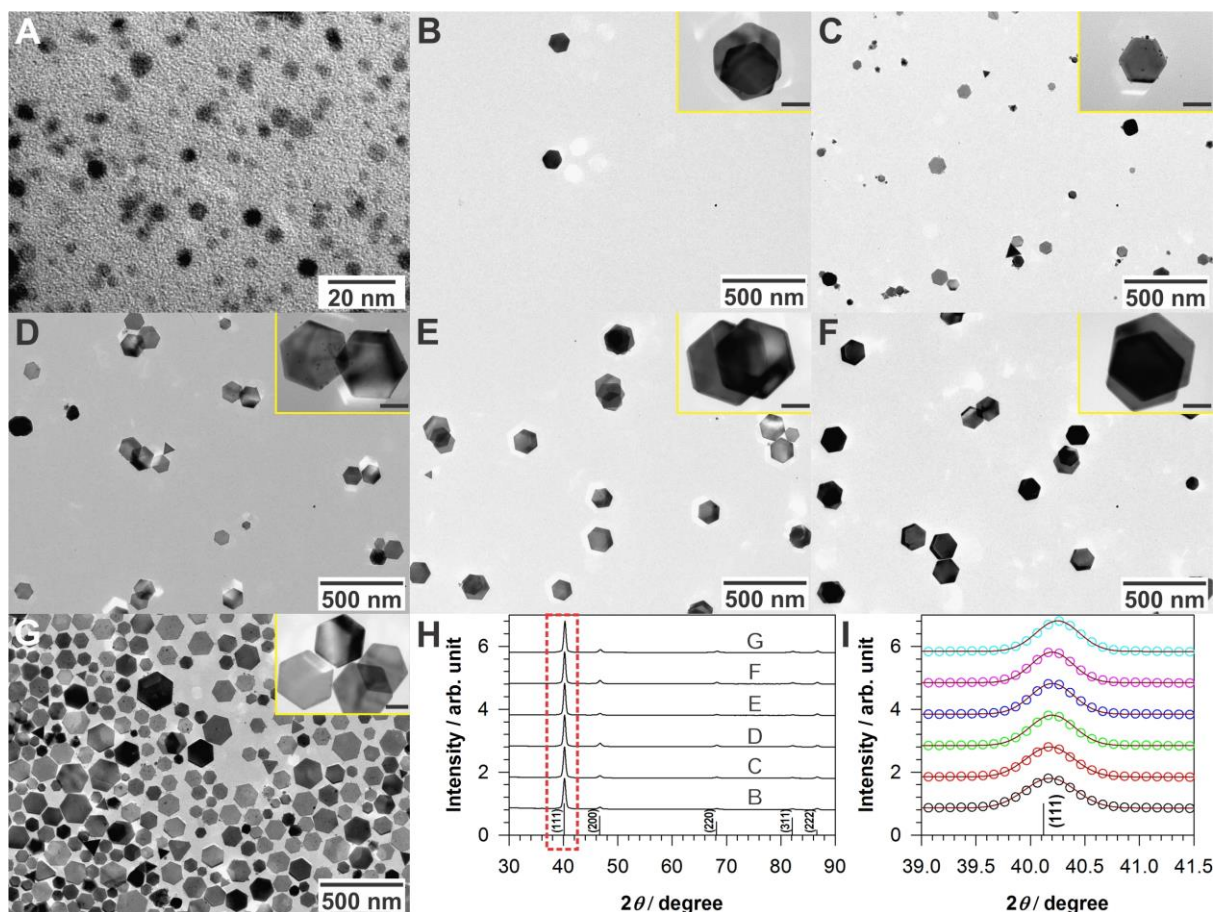


Fig. S4 (A-F) Size and shape evolution of Pd hexagonal nanoplates synthesized in the presence of PVP (PVP/Pd molar ratio: 9.6/1) and formaldehyde at 40 °C for different reaction times (A-G: 3, 12, 24, 48, 72, 96, and 120 h, respectively). Insets are corresponding higher magnification TEM images (scale bar: 50 nm). (H) XRD patterns with reference peaks for *fcc*-Pd (PDF no. 00-046-1043). (I) Extended XRD refinement in the area identified with the red dashed rectangle in H.

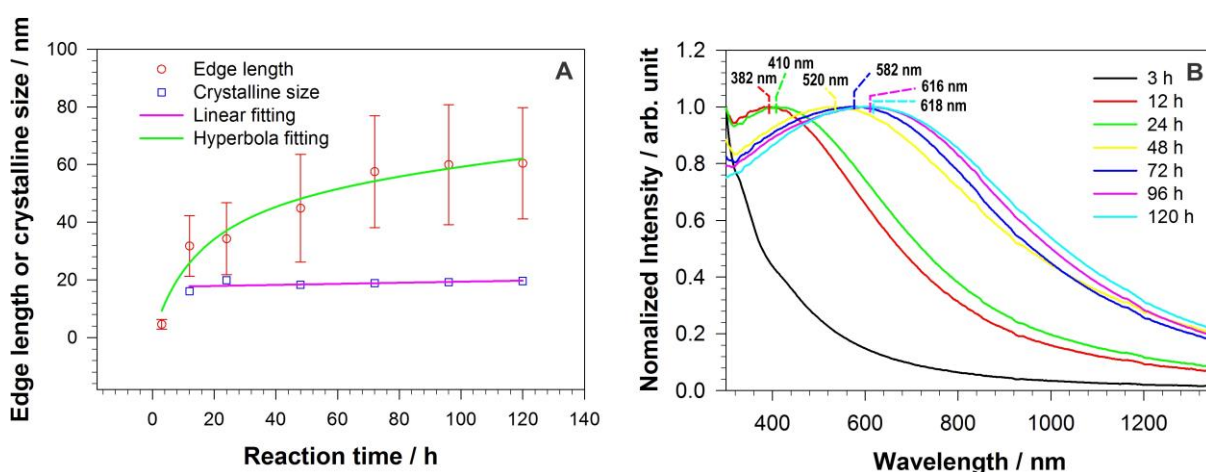


Fig. S5 (A) Edge lengths l_1 and crystalline sizes of Pd hexagonal nanoplates synthesized in the presence of PVP (PVP/Pd molar ratio: 9.6/1) and formaldehyde at 40 °C for the different times. The average edge lengths (l_1) were estimated from at least 500 nanoplates using TEM images (Fig. S4A-G). The mean crystalline sizes (D_{xrd}) were estimated from the (111) diffraction peaks (Fig. S4I) using the Scherrer formula, which represent the thickness of nanoplates. (B) UV-vis-NIR absorption spectra of Pd hexagonal nanoplates synthesized for the different reaction times.

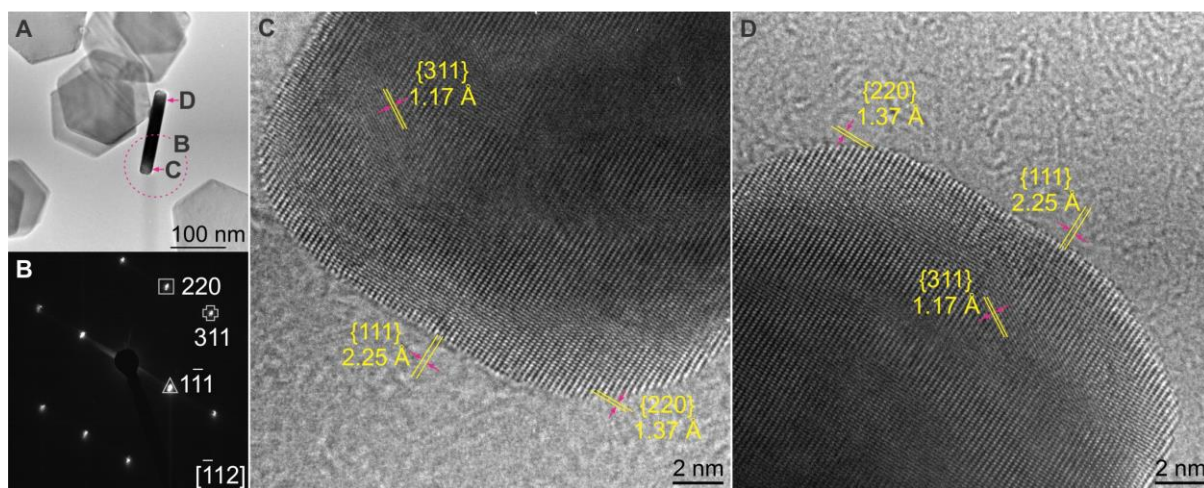


Fig. S6 (A) TEM, (C, D) Cs-corrected HRTEM images and (B) NBD pattern of individual Pd hexagonal nanoplate obtained along the $\langle 112 \rangle$ axis. The solid arrows and marked regions in the low-magnification TEM images in (A) correspond to (C, D) HRTEM images and (B) the NBD pattern. The diffraction spots in the NBD pattern in (B) and lattice fringes in HTEM images in (C) and (D) are well indexed to the $\{111\}$, $\{220\}$ and $\{311\}$ planes.

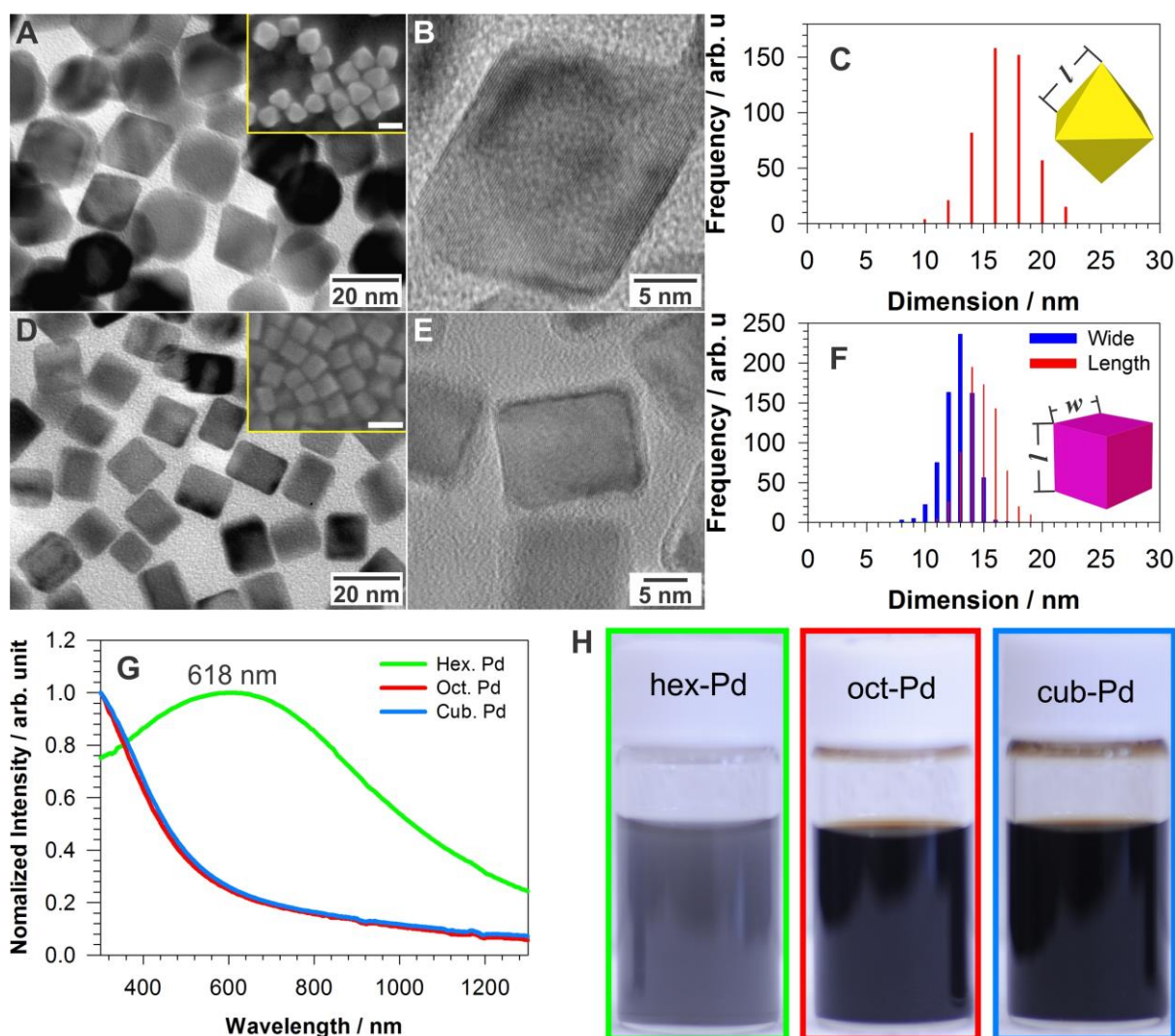


Fig. S7 (A, D) TEM, (B, E) HRTEM images and (C, F) side length distributions of (A-C) Pd octahedra and (D-F) nanocubes. Insets in (A) and (D) are corresponding SEM images (scale bar: 20 nm). (G) UV-vis-NIR absorption spectra of hex-Pd, oct-Pd and cub-Pd. (H) Dispersions of hex-Pd, oct-Pd and cub-Pd in ethanol. oct-Pd and cub-Pd exhibit non-plasmonic peaks and typical black dispersions, are deviated from hex-Pd.

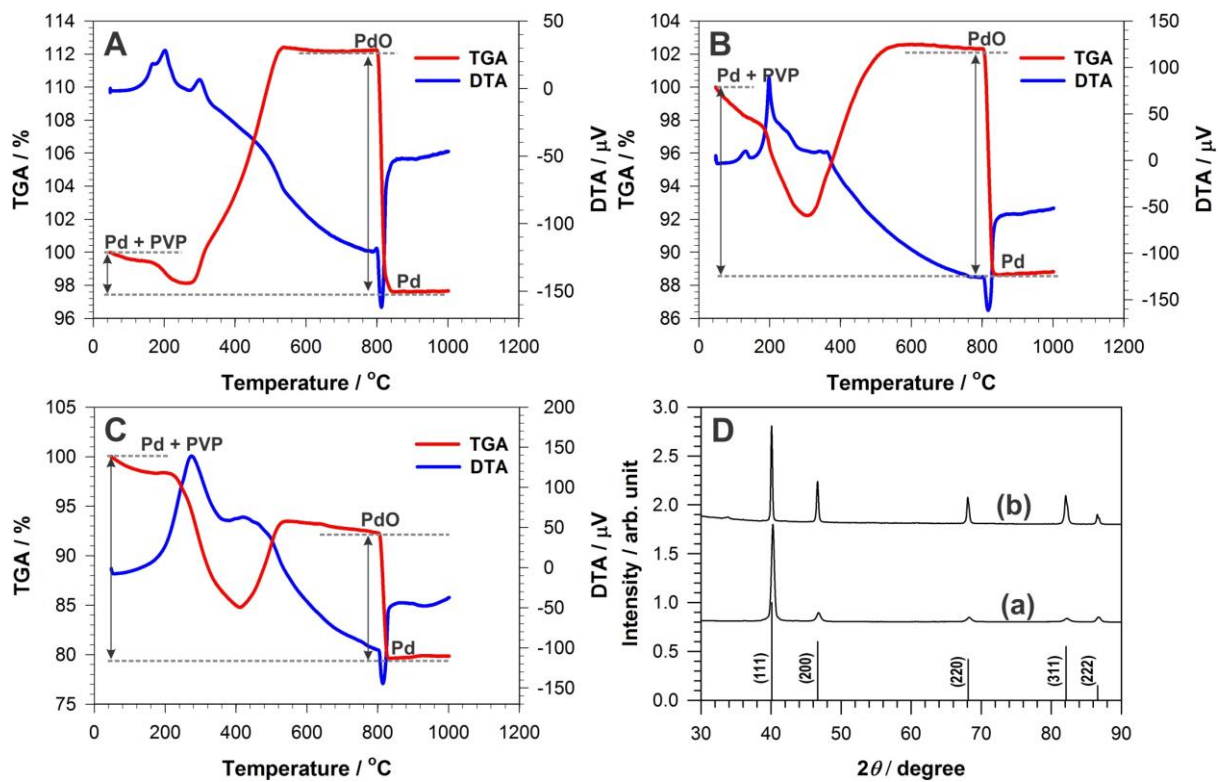


Fig. S8 (A-C) TGA/DTA of (A) hex-Pd, (B) oct-Pd, and (C) cub-Pd. All samples were heated in air at a rate of 2 °C/min and a gas flow of 50 mL/min from 50 °C to 1000 °C. (D) XRD patterns with reference peaks for *fcc*-Pd (PDF no. 00-046-1043) of hex-Pd (a) before and (b) after TGA/DTA.

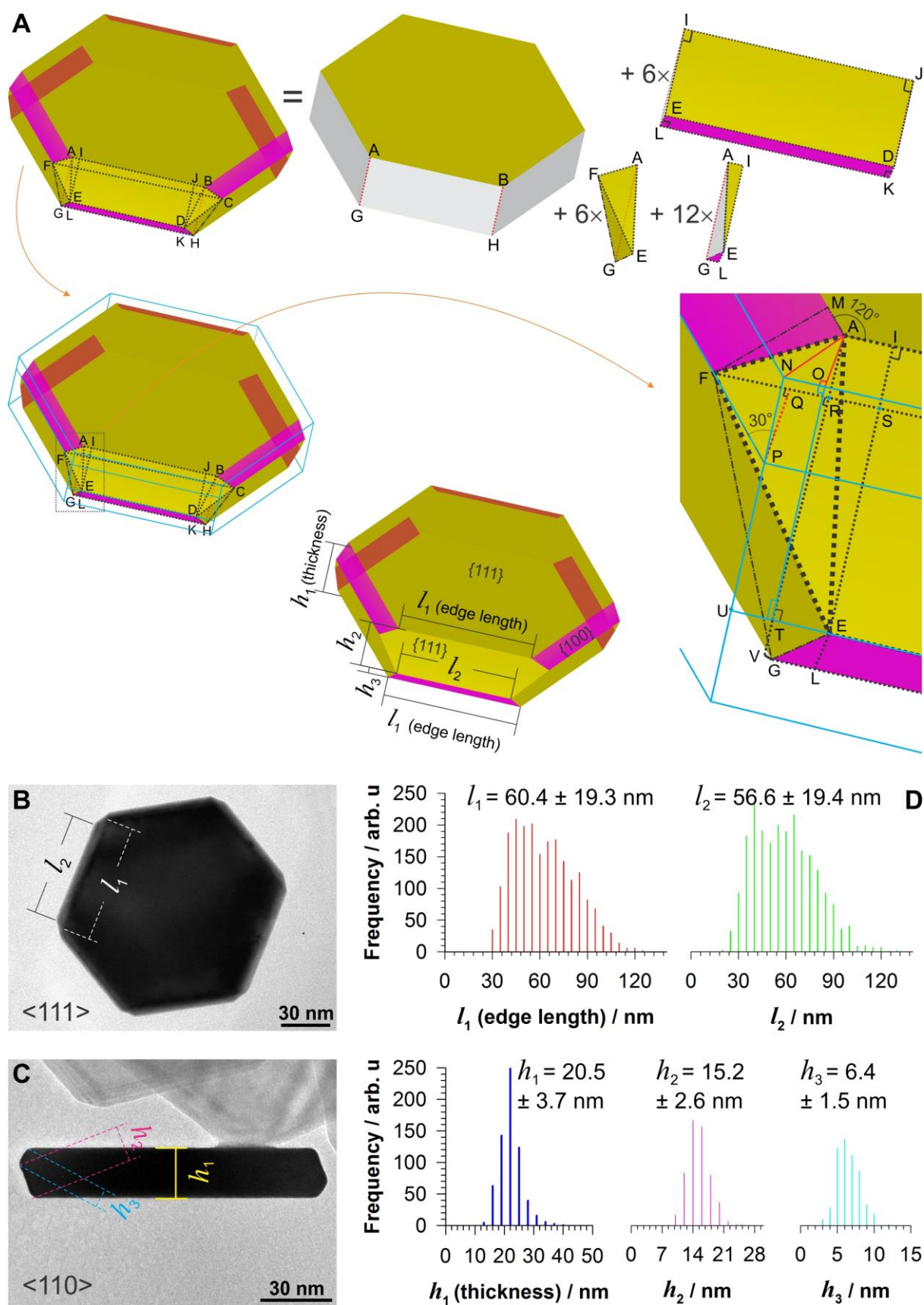


Fig. S9 (A) Schematic illustration of the Pd hexagonal nanoplate and its deconvoluted structures. (B, C) TEM images of individual Pd hexagonal nanoplates obtained along (B) the $\langle 111 \rangle$ axis and (C) the $\langle 110 \rangle$ axis. (D) Size distributions of the Pd hexagonal nanoplates synthesized over 120 h.

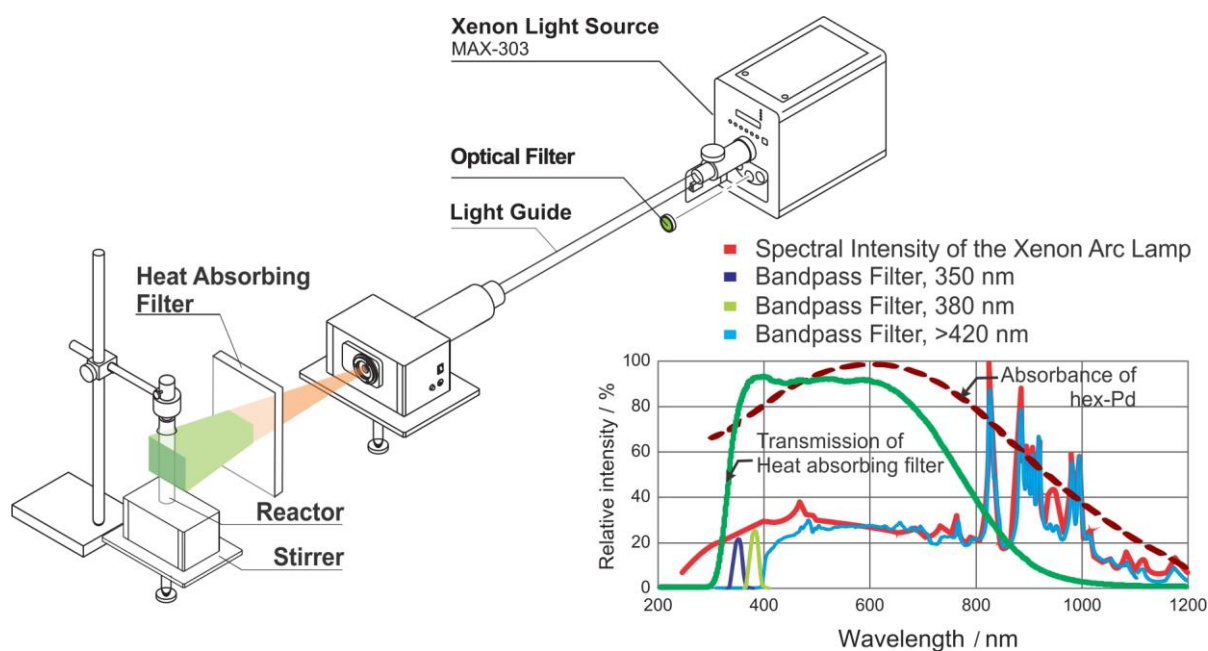


Fig. S10 Instrumentation for Suzuki coupling reactions carried out under Xenon illumination and typical spectra of the heat absorbing filter (typical transmittance: 300 – 1000 nm), optical filters, Xenon Arc Lamp and the Pd hexagonal nanoplates.

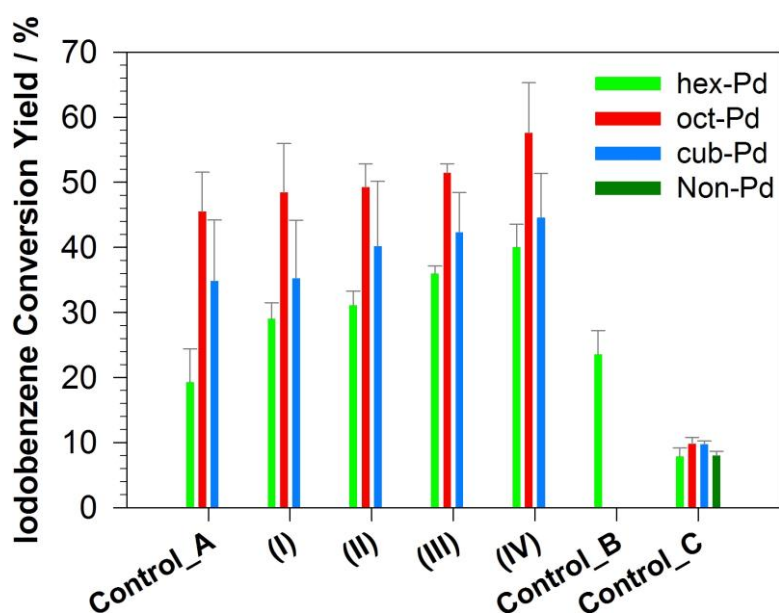


Fig. S11 Catalytic activity of hex-Pd was compared with oct-Pd and cub-Pd in Suzuki coupling reactions carried out under Xenon illumination using different light sources (I, II, III and IV; see Table 1 in the main for details). Control_A was performed without light illumination in a dark room, Control_B was performed under isothermal heating at 40 °C and Control_C was subsequently performed in solutions of the first Suzuki coupling reactions after removal of Pd NPs and without Pd NPs (Non-Pd) under light illumination with a $\lambda = 300 - 1000$ nm Xenon lamp at 176 mW cm^{-2} . The iodobenzene conversion yields in reactions Control_C are subsequent yields. All reactions were performed in an isothermal environment (25 °C) for 3 h.

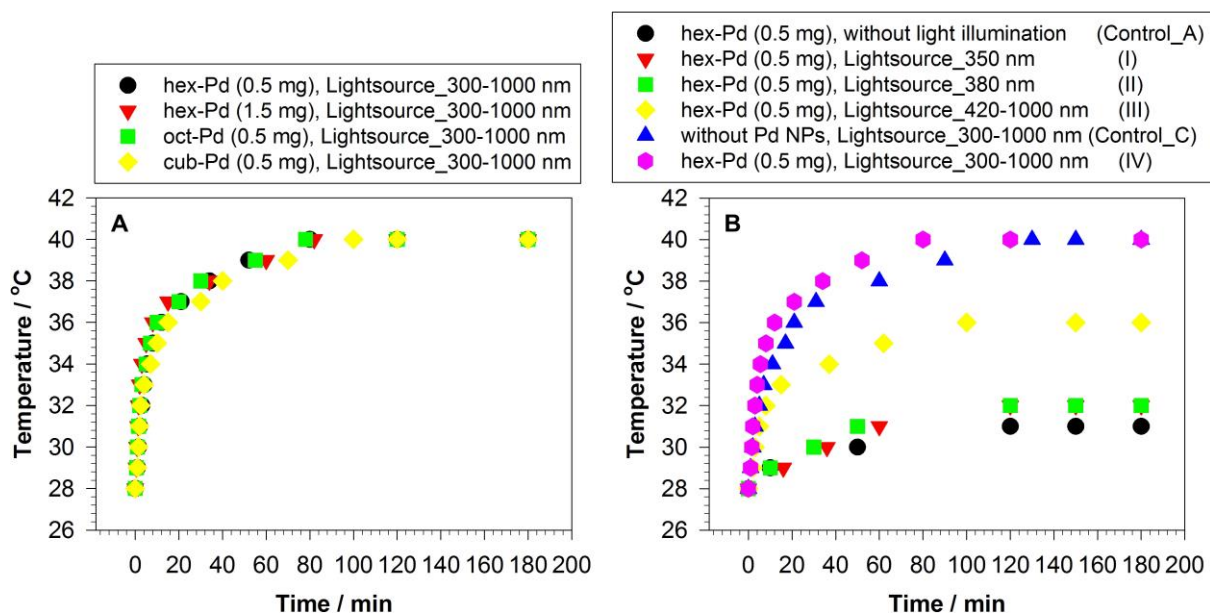


Fig. S12 Time-dependent temperature profiles of the Suzuki coupling reaction solutions. (A) The reaction solutions contain hex-Pd with two different concentrations, oct-Pd and cub-Pd. (B) The reaction solutions contain hex-Pd and are without a catalyst under Xenon illumination using different light sources. All solutions contained phenylboronic acid (0.6 mmol), K_2CO_3 (1 mmol), iodobenzene (0.3 mmol) and ethanol (4 mL). All solutions were magnetically stirred at the same rate. The final temperatures reach 31 °C for solutions without light illumination (Control_A), and 32, 32, 36 and 40 °C for solutions illuminated with the $\lambda = 350$ (I), 380 (II), 420 – 1000 (III) and 300 – 1000 nm (IV and Control_C) light sources, respectively, after 2 h. The particle concentrations of hex-Pd (0.5 mg), hex-Pd (1.5 mg), oct-Pd (0.5 mg) and cub-Pd (0.5 mg) are 8.39×10^{-2} , 2.58×10^{-1} , 9.47 and 6.81 nM, respectively.

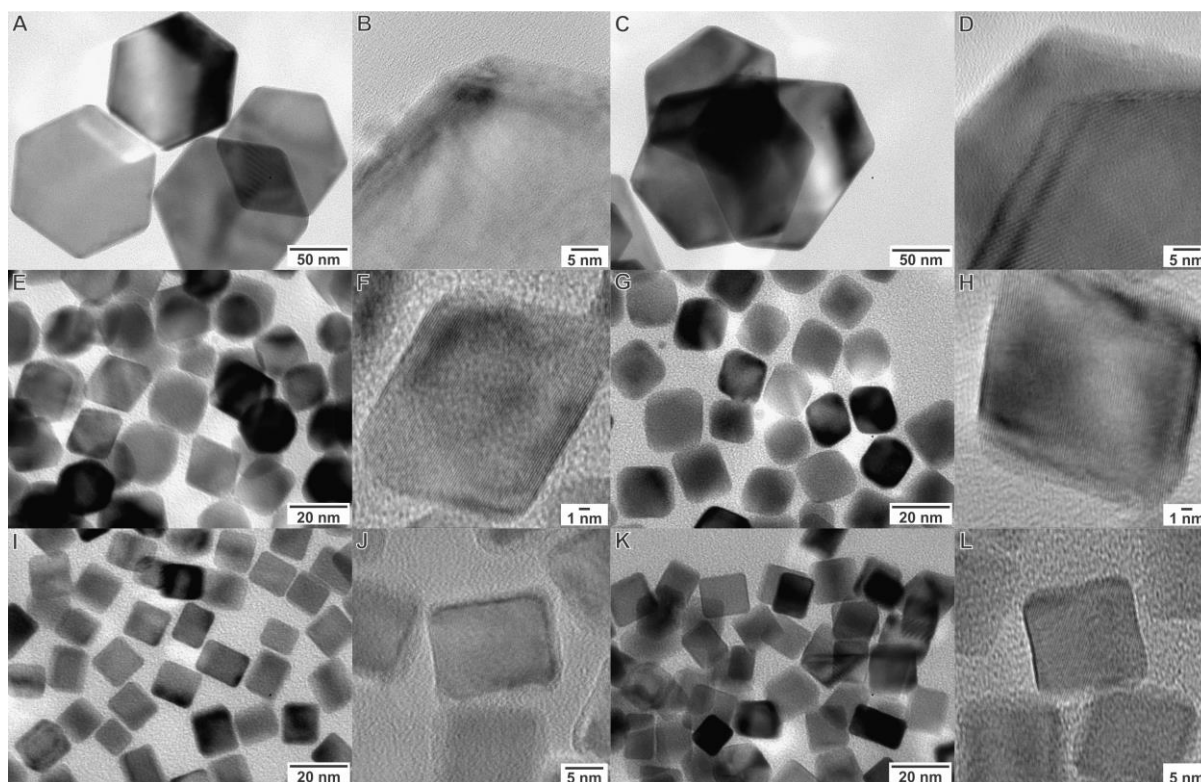


Fig. S13 (A, C, E, G, I, K) TEM and (B, D, F, H, J, L) HRTEM images of hex-Pd (A-D), oct-Pd (E-H) and cub-Pd (I-L) before (A, B, E, F, I, J) and after (C, D, G, H, K, L) the Suzuki coupling reactions under Xenon illumination of $\lambda = 300-1000$ nm Xenon lamp at 176 mW cm^{-2}

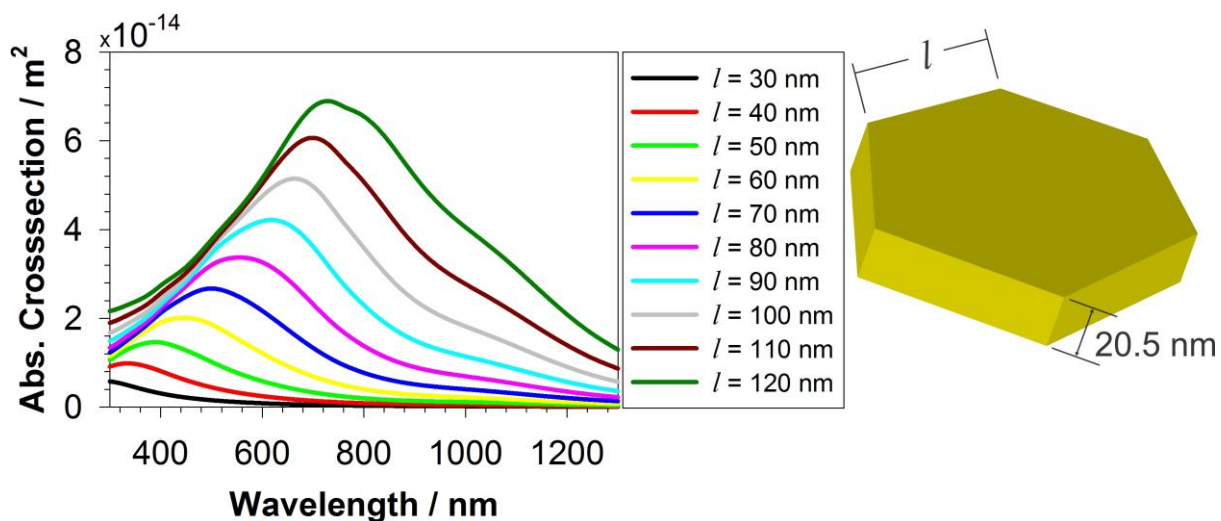


Fig. S14 Simulated absorption cross section spectra for longitudinal mode of individual regular Pd hexagonal prisms with different edge lengths ($l = 30 - 120$ nm) and a thickness of 20.5 nm. The right sketch is a model used for the simulation.

References

- 1 Y. Xia, Y. Xiong, B. Lim and S. E. S. Skrabalak, *Angew. Chem. Int. Ed.* 2009, **48**, 60-103.
- 2 Y. Xiong, I. Washio, J. Chen, H. Cai, Z-Y. Li and Y. Xia, *Langmuir* 2006, **22**, 8563-8570.
- 3 Y. Xiong and Y. Xia, *Adv. Mater.* 2007, **19**, 3385-3391.
- 4 H. Zhang, M. Jin, Y. Xiong, B. Lim and Y. Xia, *Acc. Chem. Res.* 2013, **46**, 1783-1794.
- 5 M. Jin, H. Zhang, Z. Xie and Y. Xia, *Energy & Environ. Sci.* 2012, **5**, 6352-6357.
- 6 M. Jin, H. Liu, H. Zhang, Z. Xie, J. Liu and Y. Xia, *Nano Res.* 2011, **4**, 83-91.